Cation−π Interactions with a Model for the Side Chain of Tryptophan: Structures and Absolute Binding Energies of Alkali Metal Cation−Indole Complexes†

Chunhai Ruan, Zhibo Yang, Nuwan Hallowita, and M. T. Rodgers*

Department of Chemistry, Wayne State University, Detroit, Michigan 48202

Received: July 12, 2005; In Final Form: August 31, 2005

Threshold collision-induced dissociation techniques are employed to determine bond dissociation energies (BDEs) of mono- and bis-complexes of alkali metal cations, Li^+, Na^+, K^+, Rb^+, and Cs^+, with indole, C_8H_7N. The primary and lowest energy dissociation pathway in all cases is endothermic loss of an intact indole ligand. Sequential loss of a second indole ligand is observed at elevated energies for the bis-complexes. Density functional theory calculations at the B3LYP/6-31G* level of theory are used to determine the structures, vibrational frequencies, and rotational constants of these complexes. Theoretical BDEs are determined from single point energy calculations at the MP2(full)/6-311+G(2d,2p) level using the B3LYP/6-31G* geometries. The agreement between theory and experiment is very good for all complexes except $Li^+(C_8H_7N)$, where theory underestimates the strength of the binding. The trends in the BDEs of these alkali metal cation−indole complexes are compared with the analogous benzene and naphthalene complexes to examine the influence of the extended π network and heteroatom on the strength of the cation−π interaction. The Na^+ and K^+ binding affinities of benzene, phenol, and indole are also compared to those of the aromatic amino acids, phenylalanine, tyrosine, and tryptophan to elucidate the factors that contribute to the binding in complexes to the aromatic amino acids. The nature of the binding and trends in the BDEs of cation−π complexes between alkali metal cations and benzene, phenol, and indole are examined to help understand nature's preference for engaging tryptophan over phenylalanine and tyrosine in cation−π interactions in biological systems.

Introduction

The complex three-dimensional structures that biological macromolecules assume are determined by a delicate balance of weak noncovalent interactions. Noncovalent interactions such as hydrogen bonds, hydrophobic interactions, and salt bridges have long been recognized for their importance in determining the structure and influencing the function of biological systems. In contrast, the importance of other noncovalent interactions such as cation−π,[1−5] charge−dipole,[6,7] and π stacking[8,9] interactions has only recently been recognized. In fact, gas-phase studies of cation−π interactions between a positively charged cation and an aromatic ligand with a delocalized π-electron cloud have been carried out for nearly 25 years now,[10−14] whereas the biological importance of these interactions had not been recognized until the pioneering work of Dougherty and co-workers some 10 years ago.[1,2] Since this time cation−π interactions have come to be recognized as important in protein folding and assembly,[1,2,15−19] the functioning of ionic channels in membranes,[20,21] and various molecular recognition processes.[22]

As a result of the biological relevance of cation−π interactions there has been a great deal of interest in characterizing these interactions in both model systems as well as those of direct biological relevance in an attempt to gain a better fundamental understanding of the factors that control their strength and specificity. Most of these studies have focused on interactions involving alkali metal cations, whereas organic cations[11,12] have been much less studied. Experimental measurements of the binding energies of cation−π complexes involving alkali metal cations binding to a variety of model aromatic ligands have been carried out and include benzene,[10,13,23−26] pyrrole,[28] toluene,[29] fluorobenzene,[30] aniline,[31] phenol,[32,33] anisole,[34] naphthalene,[35] and indole[32] as well as the aromatic amino acids, phenylalanine (Phe), tyrosine (Tyr), and tryptophan (Trp).[36−39] Of the simple model systems studied, benzene, phenol, and indole are of the most direct biological relevance as they correspond to the side-chain substituents of the aromatic amino acids, Phe, Tyr, and Trp. While providing detailed energetic information related to the cation−π interactions responsible for the binding in these complexes, these experimental measurements do not provide any direct structural information. Therefore, other experimental studies have sought to characterize the structures of complexes of alkali metal cation−π complexes via X-ray diffraction techniques.[40,41] Additional structural and energetic information regarding cation−π complexes has been provided by high-level theoretical calculations[2−4,25−38,42−49] such that the nature and trends in the binding have been further elucidated.

Among the aromatic amino acids, Trp is known to engage in cation−π interactions more frequently than Phe and Tyr. In an analysis of 593 high-resolution protein structures from the protein data bank (PDB), containing 230 504 amino acid residues and 2994 cation−π interactions, Gallivan and Dougherty found that 26.1% of all Trp residues present were involved in energetically significant cation−π interactions whereas Phe and Tyr were found to engage in cation−π interactions much less frequently, 10.0% and 14.3%, respectively.[50] Because the aromatic amino acids differ only in their side-chain substituent, they postulated that the reason for this preference was that in the gas phase indole binds cations more tightly than benzene

† Part of the special issue "Jack Simons Festschrift".

* Corresponding author. E-mail: mrodgers@chem.wayne.edu.

10.1021/jp053830d CCC: $30.25
Published on Web 10/21/2005

or phenol (as indicated by theoretical calculations).[1,3,4] To further validate this conclusion and provide additional insight into the reasons for nature's preference for engaging Trp in cation−π interactions over Phe and Tyr, detailed characterization of cation−π interactions between alkali metal cations and benzene, phenol, and indole is necessary.

As the side-chain substituent of Trp, indole is involved in a variety of biological processes. For instance, the distribution of amino acids in the α-helical regions of transmembrane proteins is highly nonrandom. The preference for Trp in the interface region of membrane proteins has been interpreted as indicating that Trp plays a role in their function as well as in anchoring the transmembrane protein to the lipid bilayer.[51,52] In a study of the integral membrane protein, diacylglycerol kinase (DGK), Clark et al.[53] found that five Trp residues are involved in the catalysis and that Trp is important for the alignment at the active site. Trp residues also play roles in molecular recognition processes, e.g., neurotransmitters such as acetylcholine (ACh).[1] On the basis of studies of the cation-binding abilities of synthetic receptors comprised of aromatic rings, Dougherty and Stauffer proposed a model for the biological binding sites of ACh and its derivatives. They suggested that the aromatic amino acids, particularly Trp, are critical for binding to the quaternary ammonium group of ACh such that the positive charge is surrounded and stabilized by multiple cation−π interactions.[54] Additional support for such a model for cation-binding sites comes from a study by Schiefner et al.[55] They examined the binding of glycine betaine (GB) and proline betaine (PB) by the periplasmic ligand-binding protein (ProX) and found three highly conserved Trp residues that form a rectangular aromatic box that selectively binds to a quaternary ammonium cation via cation−π interactions. Similarly, in a study of the binding of the importin β-binding (IBB) domain of importin α by importin β, Koerner et al. found that a folded IBB-helix is selectively bound and stabilized by four conserved Trp residues.[56] These studies suggest that cation−π interactions within an aromatic pocket, especially those involving Trp, provide another driving force for the lock-and-key principle in molecular recognition processes. Trp residues have also been shown to be involved in biological catalytic processes. For example, the indole side chain of Trp of several *S*-adenosyl-methionine- (SAM) dependent methyltransferases has been suggested to be involved in binding SAM by aligning the S^+-CH_3 group to a favorable position for methylation of substrates.[57]

Previous studies have carefully examined alkali metal cation−π interactions with benzene[26] and phenol[32,33] and are being extended to indole in the present study. An interesting feature of indole, the side-chain substituent of Trp, is the presence of multiple binding sites. Alkali metal cation−indole interactions may involve binding to the phenyl or pyrrolyl rings of the aromatic system or to the nitrogen atom. In contrast, cation−π complexes of indole to large organic cations may involve similar binding modes or binding to the entire extended π network of the indole moiety. Therefore, different types of cations (e.g., alkali metal cations vs organic cations) may exhibit different preferences for the available binding sites such that the relative cation affinities of the various sites may differ. Thus, elucidation of nature's preference for engaging Trp in cation−π interactions over Phe and Tyr may be enhanced by the study of cation−π complexes of indole to both alkali metal cations and complex organic cations.

Previous studies of cation−π interactions between indole and a variety of metal cations have been carried out. Dougherty and co-workers calculated the binding interactions between Na^+ and a variety of aromatic ligands including indole.[1−4] Dunbar extended these calculations to include complexes of Na^+, Mg^+, and Al^+ binding to indole and compared these results to binding to naphthalene.[49] This work showed that cation binding to the phenyl ring is favored over binding to the pyrrolyl ring and that the nitrogen binding site could not compete with the π binding sites. Ryzhov and Dunbar[32] extended these theoretical studies to include a wider variety of metal cations (Na^+, Mg^+, Al^+, K^+, Ca^+, Cr^+, Fe^+, and Mo^+) as well as experimental measurements of the binding energies via radiative association techniques.

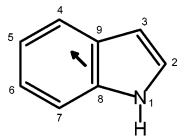

Indole
2.09 D
15.35 Å^3

Figure 1. Structure of indole. Properly scaled and oriented dipole moment (in Debye) is shown as an arrow and determined from theoretical calculations performed here. The estimated polarizability is also shown.[51]

In present work the kinetic-energy dependences of the collision-induced dissociation (CID) of alkali metal cation−indole complexes, $M^+(C_8H_7N)_x$, where $M^+ = Li^+$, Na^+, K^+, Rb^+, and Cs^+ and $x = 1$ and 2, with Xe are examined using a guided ion beam tandem mass spectrometer. The structure of indole is shown in Figure 1 along with its calculated dipole moment and estimated polarizability.[58] The kinetic-energy-dependent cross sections for the primary CID processes observed for each system are analyzed by methods developed previously.[59] The trends in and the nature of alkali metal cation binding to indole are examined and compared to other metal cations to gain a better understanding of the nature of cation−π interactions with indole. Comparisons are also made to alkali metal cations binding to benzene[26] and naphthalene[35] studied previously to examine the influence of the extended π network and nitrogen heteroatom on the binding. Trends in the alkali metal cation binding of benzene,[26] phenol,[32,33] and indole and are also compared to the aromatic amino acids[36−38] to elucidate the factors that control alkali metal cation binding and understand biology's preference for engaging Trp in cation−π interactions over Phe and Tyr.

Experimental Section

General Procedures. Cross sections for collision-induced dissociation of $M^+(C_8H_7N)_x$, where $M^+ = Li^+$, Na^+, K^+, Rb^+, and Cs^+ and $x = 1$ and 2, are measured using a guided ion beam tandem mass spectrometer that has been described in detail previously.[60] The complexes are generated in a flow tube ion source by condensation of the alkali metal cation and neutral indole ligand(s). These complexes are collisionally stabilized and thermalized by in excess of 10^5 collisions with the He and Ar bath gases such that the internal energies of the ions emanating from the source region are well described by a Maxwell−Boltzmann distribution at room temperature. The ions are effusively sampled, focused, accelerated, and focused into a magnetic sector momentum analyzer for mass analysis. Mass-selected ions are decelerated to a desired kinetic energy and focused into an octopole ion guide. The octopole passes through a static gas cell containing Xe at low pressures (~0.05−0.20 mTorr) to ensure that multiple ion−neutral collisions are improbable. The octopole ion guide acts as an efficient trap for

ions in the radial direction. Therefore, loss of scattered reactant and product ions in the octopole region is almost entirely eliminated.[61−63] Xe is used here, and in general for all of our CID measurements, because it is heavy and polarizable and therefore leads to more efficient kinetic- to internal-energy transfer in the CID process.[64−66] Products and unreacted beam ions drift to the end of the octopole where they are focused into a quadrupole mass filter for mass analysis and subsequently detected with a secondary electron scintillation detector and standard pulse counting techniques.

Ion intensities are converted to absolute cross sections using a Beers' law analysis as described previously.[67] Errors in pressure measurement and the length of the interaction region lead to ±20% uncertainties in the absolute cross-section magnitudes. Relative uncertainties are approximately ±5%.

Ion kinetic energies in the laboratory frame, E_{lab}, are converted to energies in the center of mass frame, E_{CM}, using the formula $E_{CM} = E_{lab}m/(m + M)$, where M and m are the masses of the ionic and neutral reactants, respectively. All energies reported below are in the center-of-mass frame unless otherwise noted. The absolute zero and distribution of the ion kinetic energies are determined using the octopole ion guide as a retarding potential analyzer as previously described.[67] The distribution of ion kinetic energies is nearly Gaussian with a fwhm between 0.2 and 0.4 eV (lab) for these experiments. The uncertainty in the absolute energy scale is ±0.05 eV (lab).

Because multiple ion−neutral collisions can alter the shape of CID cross sections, particularly in the threshold regions, the CID cross section for each complex was measured twice at three nominal pressures (0.05, 0.10, and 0.20 mTorr). Data free from pressure effects are obtained by extrapolating to zero reactant pressure, as described previously.[68] The zero-pressure-extrapolated cross sections subjected to thermochemical analysis are therefore the result of single bimolecular encounters.

Theoretical Calculations. To obtain model structures, vibrational frequencies, rotational constants, and energetics for neutral indole and mono- and bis-complexes of indole to the alkali metal cations, electronic structure calculations were performed using Gaussian 98.[69] Geometry optimizations were performed at the B3LYP/6-31G* level[70,71] for the $M^+(C_8H_7N)_x$ complexes, where $M^+ = Li^+$, Na^+, and K^+. For complexes containing Rb^+ and Cs^+, geometry optimizations were performed using a hybrid basis set in which the effective core potentials (ECPs) and valence basis sets of Hay and Wadt were used to describe the metal ion,[72] while the 6-31G* basis sets were used for C, H, and N atoms. As suggested by Glendening et al.,[73] a single polarization (*d*) function was added to the Hay−Wadt valence basis set for Rb and Cs with exponents of 0.24 and 0.19, respectively. Vibrational analyses of the geometry-optimized structures were performed to determine the vibrational frequencies of the optimized species for use in modeling the CID data. DFT theory, and in particular the B3LYP and B3P86 functionals, has proven very reliable for the determination of vibrational frequencies. The frequencies thus calculated were prescaled before use by a factor of 0.9804.[74−76] The prescaled vibrational frequencies are available as Supporting Information and are listed in Table 1S. Table 2S lists the rotational constants for the ground state conformations. In earlier work[29] in which we measured and calculated the strength of cation−π interactions in $M^+(C_6H_5CH_3)$ complexes, we found much better correlation between the theoretical and experimental results for energetics based on MP2(full)/6-311+G(2d,2p) theory than for B3LYP/6-311+G(2d,2p) theory. Therefore, theoretical estimates for the $M^+(C_8H_7N)_x$ bond dissociation energies (BDEs) were determined using the B3LYP/6-31G* geometries and single point energy calculations at the MP2(full)/6-311+G(2d,2p) level of theory. To obtain more accurate energetics, zero point energy (ZPE) and basis set superposition error (BSSE) corrections[77,78] were included in the calculation of theoretical BDEs.

As a result of the multiple favorable alkali metal cation-binding sites of indole, several low-energy conformations of these species are possible. Therefore, we carefully consider various possible conformations of the $M^+(C_8H_7N)_x$ complexes to determine their relative stabilities and the ground state conformations of these complexes. To obtain estimates for the barriers for interconversion of the low-energy $M^+(C_8H_7N)$ conformers, we also calculate relaxed potential energy scans for the interconversion of these species at the B3LYP/6-31G* level of theory. At each point along these scans the M^+−C2 distance was fixed, while all other parameters were allowed to relax. The highest energy structure along this reaction coordinate was then used as an initial guess for the transition state (TS) between these low-energy conformers of $M^+(C_8H_7N)$. A TS optimization of this structure was then performed at the B3LYP/6-31G* level of theory (and confirmed to be a TS between the π5 and π6 conformers), while its energy was characterized at the MP2(full)/6-311+G(2d,2p) level of theory including BSSE and ZPE corrections.

To more clearly visualize the electronic properties of indole and understand its preferences for various binding sites, we also calculated an electrostatic potential map for neutral indole. The process involves calculation of the interaction between a +1 probe charge and every part of the electron density cloud of indole. The electrostatic potential is then mapped onto an isosurface of the total SCF electron density (0.005 au for the map generated in this work). The electrostatic potential map generated via this procedure was then color-coded according to its potential with the regions of most negative electrostatic potential shown in red and those with the most positive electrostatic potential shown in blue.

Thermochemical Analysis. The threshold regions of the CID cross sections are modeled using eq 1

$$\sigma(E) = \sigma_0 \sum_i g_i (E + E_i - E_0)^n / E \qquad (1)$$

where σ_0 is an energy-independent scaling factor, E is the relative translational energy of the reactants, E_0 is the threshold for reaction of the ground electronic and ro-vibrational state, and n is an adjustable parameter that describes the efficiency of kinetic- to internal-energy transfer.[79] The summation is over the ro-vibrational states of the reactant ions, i, where E_i is the excitation energy of each ro-vibrational state and g_i is the population of those states ($\sum g_i = 1$). The relative reactivity of all ro-vibrational states, as reflected by σ_0 and n, is assumed to be equivalent.

The Beyer−Swinehart algorithm[80−82] is used to evaluate the density of the ro-vibrational states, and the relative populations, g_i, are calculated by an appropriate Maxwell−Boltzmann distribution at 298 K, the internal temperature of the reactants. The average internal energies at 298 K of neutral indole and the $M^+(C_8H_7N)_x$ complexes are also given in Table 1S. We estimated the sensitivity of our analysis to the deviations from the true frequencies by increasing and decreasing the prescaled frequencies by 10% to encompass the range of average scaling factors needed to bring calculated frequencies into agreement with experimentally determined frequencies.[83,84] The corresponding change in the average vibrational energy is taken to be an estimate of one standard deviation of the uncertainty in

vibrational energy (Table 1S) and is included in the uncertainties listed with the E_0 and E_0(PSL) values.

We also consider the possibility that collisionally activated complex ions do not dissociate on the time scale of our experiment ($\sim 10^{-4}$ s) by including statistical theories for unimolecular dissociation, specifically Rice−Ramsperger−Kassel−Marcus (RRKM) theory, into eq 1 as described in detail elsewhere.[59,85] This requires sets of ro-vibrational frequencies appropriate for the energized molecules and the transition states (TSs) leading to dissociation. The former sets are given in Tables 1S and 2S, whereas we assume that the TSs are loose and product-like because the interaction between the alkali metal cation and indole ligand is largely electrostatic. In this case, the TS vibrations used are the frequencies corresponding to the products, indole and $M^+(C_8H_7N)_{x-1}$, which are also found in Table 1S. The transitional frequencies, those that become rotations of the completely dissociated products, are treated as rotors, a treatment that corresponds to a phase space limit (PSL) and is described in detail elsewhere.[59]

The model represented by eq 1 is expected to be appropriate for translationally driven reactions[86] and has been found to reproduce CID cross sections well. The model of eq 1 is convoluted with the kinetic-energy distributions of both reactants, and a nonlinear least-squares analysis of the data is performed to give optimized values for the parameters σ_0, E_0, and n. The error associated with the measurement of E_0 is estimated from the range of threshold values determined for the eight zero-pressure-extrapolated data sets, variations associated with uncertainties in the vibrational frequencies (scaling as discussed above), and the error in the absolute energy scale, 0.05 eV (lab). For analyses that include the RRKM lifetime analysis, the uncertainties in the reported E_0(PSL) values also include the effects of increasing and decreasing the time assumed available for dissociation ($\sim 10^{-4}$ s) by a factor of 2.

Equation 1 explicitly includes the internal energy of the ion, E_i. All energy available is treated statistically because the ro-vibrational energy of the reactants is redistributed throughout the reactant ion upon collision with Xe. Because the CID processes examined here are simple noncovalent bond cleavage reactions, the E_0(PSL) values determined by analysis with eq 1 can be equated to 0 K BDEs.[87,88]

Results

Cross Sections for Collision-Induced Dissociation. Experimental cross sections were obtained for the interaction of Xe with 10 $M^+(C_8H_7N)_x$ complexes, where $M^+ = Li^+$, Na^+, K^+, Rb^+, and Cs^+ and $x = 1$ and 2. Figure 2 shows representative data for the $Na^+(C_8H_7N)_x$ complexes. The other $M^+(C_8H_7N)_x$ complexes exhibit similar behavior and are shown in Figure 1S in the Supporting Information. Over the collision energy range studied, two types of processes are observed: the sequential loss of intact indole ligands and ligand exchange with Xe. The most favorable process is the loss of a single intact indole ligand in the CID reactions 2

$$M^+(C_8H_7N)_x + Xe \rightarrow M^+(C_8H_7N)_{x-1} + C_8H_7N + Xe \quad (2)$$

Dissociation of a second indole ligand is observed for the bis-complexes at elevated energies. The shape of the CID cross sections confirms that these products are formed sequentially from the primary CID product, i.e., the cross section for formation of $M^+(C_8H_7N)$ begins to decline as the secondary product, M^+, begins to appear. Ligand exchange to form M^+-Xe is observed for the $Na^+(C_8H_7N)$ complex. It is likely that this process occurs for all complexes but that the signal-to-noise in the other experiments was not sufficient to differentiate the M^+Xe product from background noise.

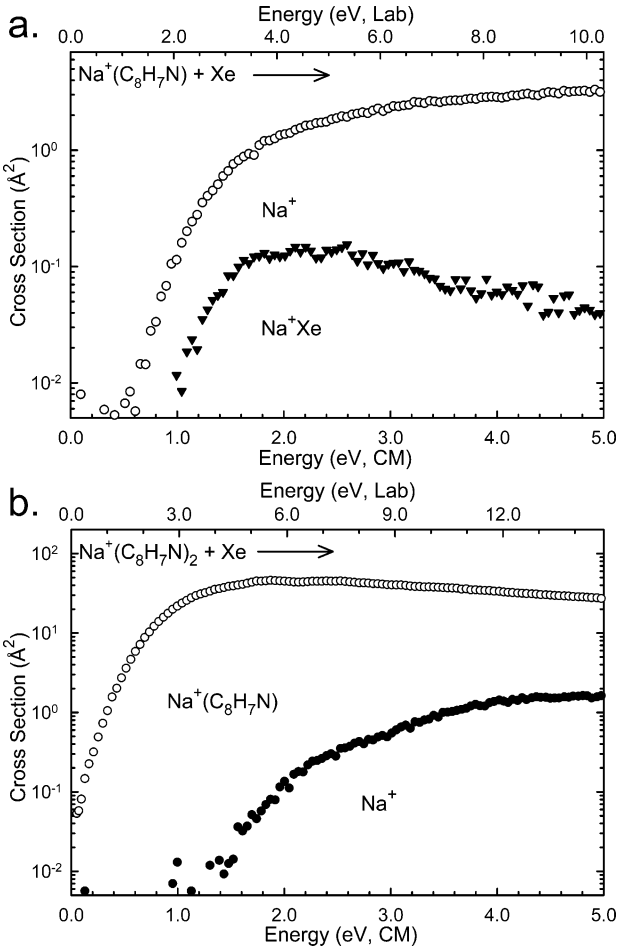

Figure 2. Cross sections for collision-induced dissociation of $Na^+(C_8H_7N)_x$ complexes with Xe as a function of collision energy in the center-of-mass frame (lower x-axis) and laboratory frame (upper x-axis), where $x = 1$ and 2, parts a and b, respectively. Data are shown for a Xe pressure of 0.2 mTorr.

Threshold Analysis. The model of eq 1 was used to analyze the thresholds for reactions 2 in 10 $M^+(C_8H_7N)_x$ systems. The results of these analyses are provided in Table 1, and representative results for the $Na^+(C_8H_7N)_x$ complexes are shown in Figure 3. The analyses for the other $M^+(C_8H_7N)_x$ complexes are shown in Figure 2S in the Supporting Information. In all cases, the experimental cross sections for CID reactions 2 are accurately reproduced using a loose PSL TS model.[59] Previous work has shown that this model provides the most accurate assessment of the kinetic shifts for CID processes of electrostatically bound ion−molecule complexes.[59] Good reproduction of the data is obtained over energy ranges exceeding 1.5 eV and cross section magnitudes of at least a factor of 100. Table 1 also lists values of E_0 obtained without including the RRKM lifetime analysis. Comparison of these values with the E_0(PSL) values provides a measure of the kinetic shift associated with the finite experimental time window, which should correlate with the density of states at threshold. The kinetic shifts decrease with increasing size of the alkali metal cation for both the mono- and bis-complexes in accordance with the measured thresholds for dissociation in these systems. The kinetic shifts are also larger for the bis-complexes than the corresponding mono-complexes as a result of the larger number of vibrational degrees of freedom, and thus density of states, in the former complexes.

TABLE 1: Fitting Parameters of Eq 1, Threshold Dissociation Energies at 0 K, and Entropies of Activation at 1000 K of $M^+(C_8H_7N)_x$[a]

species	σ_0[b]	n[b]	E_0[c] (eV)	E_0(PSL) (eV)	kinetic shift (eV)	$\Delta S^{\ddagger}$(PSL) (J mol^{-1} K^{-1})
$Li^+(C_8H_7N)$	13.0 (2.6)	1.68 (0.19)	2.43 (0.08)	2.12 (0.09)	0.31	47 (2)
$Na^+(C_8H_7N)$	2.2 (0.1)	1.29 (0.03)	1.29 (0.04)	1.25 (0.03)	0.04	42 (3)
$K^+(C_8H_7N)$	4.4 (0.2)	0.71 (0.10)	1.04 (0.05)	1.03 (0.04)	0.01	37 (3)
$Rb^+(C_8H_7N)$	3.3 (0.1)	1.13 (0.02)	0.94 (0.04)	0.93 (0.03)	0.01	31 (2)
$Cs^+(C_8H_7N)$	9.2 (0.2)	0.89 (0.01)	0.86 (0.03)	0.85 (0.03)	0.01	26 (2)
$Li^+(C_8H_7N)_2$	17.0 (0.6)	1.05 (0.01)	1.57 (0.09)	1.24 (0.05)	0.33	37 (5)
$Na^+(C_8H_7N)_2$	50.4 (2.7)	1.10 (0.08)	1.14 (0.06)	1.01 (0.03)	0.13	39 (5)
$K^+(C_8H_7N)_2$	101.6 (3.0)	0.95 (0.06)	0.91 (0.06)	0.79 (0.03)	0.12	17 (5)
$Rb^+(C_8H_7N)_2$	39.7 (2.3)	1.07 (0.10)	0.87 (0.06)	0.76 (0.03)	0.11	17 (5)
$Cs^+(C_8H_7N)_2$	15.4 (1.4)	1.31 (0.04)	0.79 (0.07)	0.72 (0.03)	0.07	17 (5)

[a] Uncertainties are listed in parentheses. [b] Average values for loose PSL transition state. [c] No RRKM analysis.

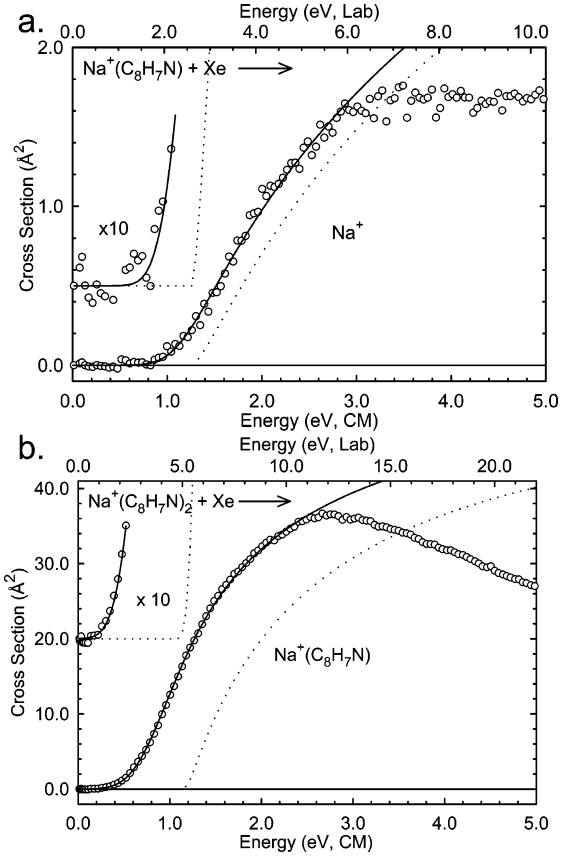

Figure 3. Zero-pressure-extrapolated cross sections for collision-induced dissociation of $Na^+(C_8H_7N)_x$ complexes with Xe in the threshold region as a function of kinetic energy in the center-of-mass frame (lower *x*-axis) and laboratory frame (upper *x*-axis), where $x = 1$ and 2, parts a and b, respectively. The solid lines show the best fits to the data using eq 1 convoluted over the neutral and ion kinetic- and internal-energy distributions. The dotted lines show the model cross sections in the absence of experimental kinetic-energy broadening for reactants with an internal energy corresponding to 0 K.

The entropy of activation, $\Delta S^{\ddagger}$, is a measure of the looseness of the TS and also a reflection of the complexity of the system. It is largely determined by the molecular parameters used to model the energized molecule and the TS for dissociation but also depends on the threshold energy. The $\Delta S^{\ddagger}$(PSL) values at 1000 K are listed in Table 1 and vary from 26 to 47 J/K mol for the mono-complexes and 17 to 39 J/K mol for the bis-complexes. The values are the largest for the Li^+ complexes and decrease with increasing size of the cation such that the trends in the $\Delta S^{\ddagger}$ values parallel the measured thresholds for dissociation in these systems.

Theoretical Results. Theoretical structures for indole and the mono- and bis-complexes of indole with Li^+, Na^+, K^+, Rb^+, and Cs^+ were calculated at the B3LYP/6-31G* level of theory as described above. Theoretical estimates for the BDEs of the $M^+(C_8H_7N)_x$ complexes were determined using the B3LYP/6-31G* geometries and single point energy calculations at the MP2(full)/6-311+G(2d,2p) level of theory including ZPE and BSSE corrections. These results are listed in Table 2 along with other theoretical results found in the literature.[32,49] Table 3 provides key geometrical parameters of the ground state geometries for each of these species.

The electrostatic potential map of indole was calculated as described in the Theoretical Calculations section and is shown in Figure 4. As can be seen in the figure, the regions of greatest electron density (color-coded in red) occur above and below the plane of the molecule as expected based upon the delocalized π electron density of the aromatic system. In contrast, the most electropositive regions (color-coded in blue) occur near the plane of the molecule around the hydrogen atoms. The electron density is fairly isotropic and greatest above the phenyl ring. In contrast, the electron density above the pyrrolyl ring is much less isotropic and somewhat reduced as a result of the presence of the nitrogen heteroatom. On the basis of the electrostatic potential map, stable binding modes of the alkali metal cations to indole might be expected to occur above the phenyl ring and pyrrolyl ring and to the nitrogen atom. Therefore, each of these potential binding sites was probed.

Alkali Metal Cation Binding. Two stable conformers, designated π5 and π6, were found for the $M^+(C_8H_7N)$ complexes. The π6 conformer corresponds to the ground state conformation for all alkali metal cations. In the π6 conformer the metal cation sits above the phenyl ring and binds to its π cloud. In the π5 conformer the metal cation sits above the pyrrolyl ring and binds to its π cloud. The B3LYP/6-31G* geometry optimized structures of the π5 and π6 conformers of the $Na^+(C_8H_7N)$ complex are shown in Figure 5. Stable minima corresponding to the π5 conformer were only found for the Li^+, Na^+, and K^+ complexes. The strength of binding in these π5 complexes is weaker than in the corresponding π6 complexes by 20.2, 12.0, and 7.6 kJ/mol for Li^+, Na^+, and K^+, respectively. Attempts to calculate stable π5 conformers for Rb^+ and Cs^+ complexes always converged to the energetically more favorable π6 conformers. Attempts were also made to calculate stable conformers of the $M^+(C_8H_7N)$ complexes in which the alkali metal cation binds to the nitrogen atom. However, the complexes always converge to the energetically more favorable π5 conformers for Li^+, Na^+, and K^+ and the π6 conformers for Rb^+ and Cs^+.

TABLE 2: Enthalpies of Metal-Ion Binding to Indole, Benzene, Phenol, and Naphthalene at 0 K in kJ/mol

	experiment (TCID)				literature		theory (L = C_8H_7N)			
complex	L = C_8H_7N[a]	L = C_6H_6[b]	L = C_6H_5OH[c]	L = $C_{10}H_8$[d]	L = C_8H_7N[e]	conformer	D_e[f]	D_0[f,g]	$D_{0,BSSE}$[f,h]	literature
$Li^+(L)$	204.5 (8.7)	161.1 (13.5)	178.5 (16.1)	187.2 (16.4)		π6	194.3	186.4	175.8	
						π5	173.2	166.1	155.6	
						TS	162.4	157.2	148.7	
$Na^+(L)$	121.1 (2.9)	92.6 (5.8)	102.3 (3.4)	107.1 (5.0)		π6	131.8	127.4	116.4	150.6[i]
					137.7 (13.7)					
		88.3 (4.3)[j]	98.5 (3.4)[j]							136.5[k]
						π5	118.4	115.1	104.4	126.8[i]
$K^+(L)$	99.8 (3.9)	73.3 (3.8)	74.0 (3.4)	80.9 (5.1)	104.6 (10.5)	π6	104.8	101.5	95.1	86.9[l]
						π5	96.8	94.1	87.5	
$Rb^+(L)$[m]	90.1 (2.9)	68.5 (3.8)	68.7 (4.4)	73.0 (4.9)		π6	96.8	94.1	75.4	
$Cs^+(L)$[m]	82.3 (2.9)	64.6 (4.8)	65.3 (4.9)	69.3 (5.4)		π6	89.1	86.3	67.2	
$Li^+(L)_2$	119.6 (4.8)	104.2 (6.8)	114.5 (3.2)	116.8 (4.0)		π6a	151.4	148.3	125.3	
						π6s	146.7	144.0	121.6	
						π5a	141.1	138.6	118.8	
$Na^+(L)_2$	97.4 (2.9)	80.0 (5.8)	81.6 (3.1)	91.1 (2.5)		π6a	116.3	112.9	95.9	
						π6s	114.4	111.5	94.7	
$K^+(L)_2$	79.4 (2.9)	67.5 (6.8)	68.4 (3.2)	74.8 (3.4)		π6a	92.8	90.2	78.7	
						π6s	92.6	90.0	78.5	
$Rb^+(L)_2$[m]	73.3 (2.9)	62.7 (7.7)	63.7 (4.4)	69.6 (4.0)		π6a	89.4	87.1	74.5	
						π6s	87.3	85.0	72.2	
$Cs^+(L)_2$[m]	68.5 (2.9)	58.8 (7.7)	60.4 (4.0)	65.1 (3.3)		π6a	77.2	75.3	64.3	
						π6s	76.7	74.7	63.9	

[a] Present results, uncertainties are listed in parentheses. [b] Reference 26. [c] Reference 33. [d] Reference 35. [e] Radiative association, ref 32. [f] Present results, calculated at the MP2(full)/6-311+G(2d,2p)//B3LYP/6-31G*. [g] Including ZPE corrections with B3LYP/6-31G* frequencies scaled by 0.9804. [h] Also includes BSSE corrections. [i] Reference 49, D_0, MP2/6-31G*//HF/6-31G*. [j] Reference 25. [k] Reference 4, D_e, HF/6-31G**. [l] B3LYP, including ZPE corrections, ref 32. [m] The Hay−Wadt ECP/valence basis set was used for the alkali metal cation, as described in the text, and the 6-31G* and 6-311+G(2d,2p) basis set were used for C, N, and H in geometry optimizations and single point energy calculations, respectively.

TABLE 3: Geometrical Parameters of Ground State B3LYP/6-31G* Optimized Structures of C_8H_7N and $M^+(C_8H_7N)_x$ Complexes[a]

species	conformer	$M^+-R_\perp$ (Å)	M^+-R_C (Å)	offset (Å)	C−C (Å)	C−H (Å)	C−H OOP− (deg)
C_8H_7N					1.411	1.087	0.000
$Li^+(C_8H_7N)$	π6	1.847	1.852	0.139	1.420	1.085	0.564
$Na^+(C_8H_7N)$	π6	2.339	2.346	0.179	1.418	1.086	0.731
$K^+(C_8H_7N)$	π6	2.822	2.826	0.161	1.416	1.086	0.731
$Rb^+(C_8H_7N)$	π6	3.119	3.126	0.204	1.415	1.086	2.374
$Cs^+(C_8H_7N)$	π6	3.392	3.400	0.225	1.415	1.086	2.062
$Li^+(C_8H_7N)_2$	π6a	2.038	2.056	0.273	1.417	1.085	0.783
$Na^+(C_8H_7N)_2$	π6a	2.426	2.437	0.223	1.417	1.086	1.543
$K^+(C_8H_7N)_2$	π6a	2.884	2.888	0.165	1.415	1.086	1.806
$Rb^+(C_8H_7N)_2$	π6a	3.182	3.175	0.311	1.415	1.086	1.902
$Cs^+(C_8H_7N)_2$	π6a	3.457	3.450	0.240	1.414	1.086	1.833

[a] $M^+-R_\perp \equiv$ perpendicular distance between the alkali metal cation and the phenyl ring of indole. $M^+-R_C \equiv$ distance between the alkali metal cation and the centoid of the phenyl ring. Offset ≡ parallel distance from the alkali metal cation to the centroid of the phenyl ring. C−H OOP− ≡ average C−H out of plane angle.

To estimate the barrier to interconversion between the π5 and π6 conformers of the Li^+, Na^+, and K^+ complexes, relaxed potential energy scans for the interconversion of these species were calculated as described in the Theoretical Calculations section and shown in Figure 6. At each point along these scans the M^+-C2 distance was fixed, while all other parameters were allowed to relax. The highest energy structure along this reaction coordinate was then used as an initial guess for the TS between these low-energy conformers of $M^+(C_8H_7N)$. However, we were only able to find a true TS for the $Li^+(C_8H_7N)$ complex. Multiple attempts to characterize the TS for the Na^+ and K^+ complexes were unsuccessful. Relative to the π6 conformer, the TS for $Li^+(C_8H_7N)$ complex lies 27.1 and 6.9 kJ/mol higher in energy than the π6 and π5 conformers, respectively. The energetics associated with the TS are also summarized in Table 2. Failure to find the TS for the Na^+ and K^+ systems suggests that the barriers to interconversion decrease as the strength of the binding interaction decreases. This also suggests that the barrier to interconversion becomes small enough for Rb^+ and Cs^+ that these complexes do not get trapped in the π5 well during the geometry optimization such that the ground state structure is always found for these alkali metal cations.

The similar energies of the π6 and π5 conformers calculated for the Li^+, Na^+, and K^+ systems suggest that the ion beams generated under our experimental conditions may be composed of a mixture of both species. Because the technique used here to measure the BDEs is a threshold technique, our results should correlate with the least strongly bound conformer produced in reasonable abundance. The 298 K Maxwell−Boltzmann populations of the π5 conformers generated should represent ~0.03%, 0.8%, and 4.5% of the total ion population for the Li^+, Na^+, and K^+ complexes, respectively. Because the relative populations of the π5 conformers are quite small for these systems, they are unlikely to influence the threshold determination, particularly for the Li^+ and Na^+ complexes.

The distortion of the indole molecule that occurs upon binding to the alkali metal cation is minor. The change in geometry is largest for the complex to Li^+ and decreases with increasing size of the alkali metal cation. In the π6 conformer the C−C bond lengths of the phenyl ring were found to increase by

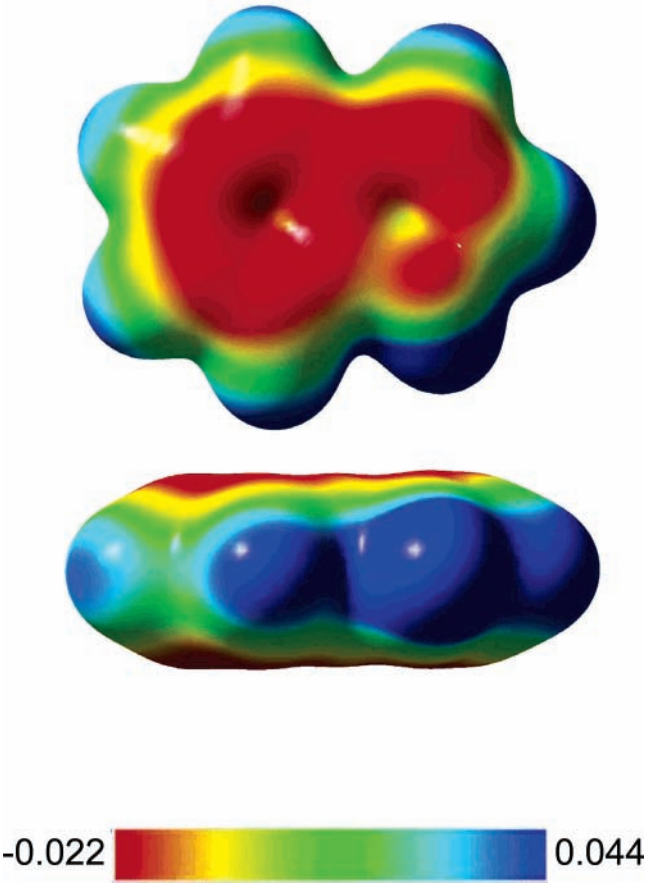

Figure 4. Electrostatic potential map of indole at an isosurface of 0.005 au of the total SCF electron density. Two views are shown. In the view from above, indole is oriented as in Figure 1. The view from the side is obtained by rotating the top view such that the nitrogen atom points out of the plane of the page.

0.004−0.009 upon complexation to the alkali metal cation as compared to the free indole ligand (Table 3). In contrast, the aromatic C−H bond lengths decrease by 0.001−0.003 Å upon complexation. As summarized in Table 3, the $M^+-R_\perp$ and M^+-R_C distances[89] are found to increase as the size of the alkali metal cation increases for both mono- and bis-complexes. These distances are also found to increase on going from a mono- to the corresponding bis-complex.

Several low-energy conformations are available to the bis-complexes. Clearly, the most stable conformers have the alkali metal cation sandwiched between the phenyl rings of the indole ligands. However, the magnitude of ligand−ligand repulsion varies with the relative orientations of the indole ligands. Ligand−ligand repulsion should be minimized when the indole molecules are parallel and oriented anti with respect to one another such that the complex has a near zero dipole moment. This conformation is designated here as the π6a conformer as shown in Figure 5 for the $Na^+(C_8H_7N)_2$ complex and corresponds to the ground state geometry of the bis-complexes. Upon optimization the indole ligands relax slightly such that the indole ligands are not quite antiparallel and become "skewed" with respect to one another. The degree of skew in the π6a conformers is smallest for the Li^+ complex and increases slightly with the size of the alkali metal cation.

To estimate the barrier to free rotation of the indole ligands in the bis-complexes, optimizations were performed for the $Li^+(C_8H_7N)_2$ complex with various degrees of rotation of the aromatic rings. The least stable conformation of this complex corresponded to the indole ligands being oriented syn with

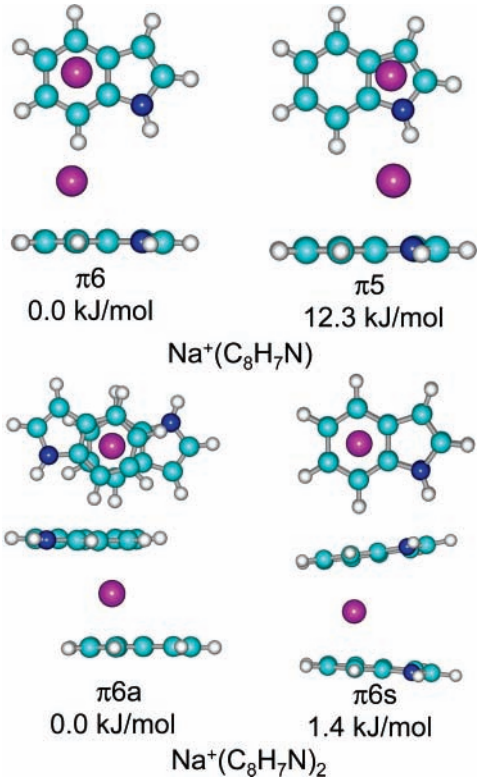

Figure 5. B3LYP/6-31G* optimized geometries of $Na^+(C_8H_7N)$ and $Na^+(C_8H_7N)_2$. Two views of each conformer are shown.

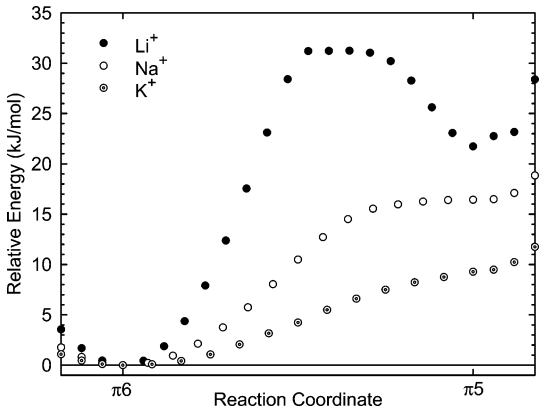

Figure 6. B3LYP/6-31G* relaxed potential energy scans for interconversion of the π6 and π5 conformers of $M^+(C_8H_7N)$ at 0 K, where $M^+ = Li^+$, Na^+, and K^+.

respect to one another and is designated here as the π6s conformer. Thus, the π6s conformers were calculated for all of the bis-complexes. Upon optimization, repulsive interactions between the pyrrolyl rings, which are not directly interacting with the alkali metal cation, cause the indole ligands to fan out from a parallel orientation. Clearly, the repulsive interactions are greatest between the nitrogen atoms as they fan out to a greater extent than the other atoms in the pyrrolyl ring. The π6s conformer of the $Na^+(C_8H_7N)_2$ complex is shown in Figure 5. The extent to which the two indole ligands deviate from parallel in the π6s conformers is smallest for the Li^+ complex and increases with the size of the alkali metal cation. The π6s conformers were found to be of similar energy but slightly less stable than the ground state π6a complexes. Therefore, at room temperature the π6 bis-complexes should have sufficient internal energy to freely interconvert (see Table 1S) between any of the low-energy conformations in which the alkali metal cation binds to the phenyl rings of both indole ligands. Thus, it seems

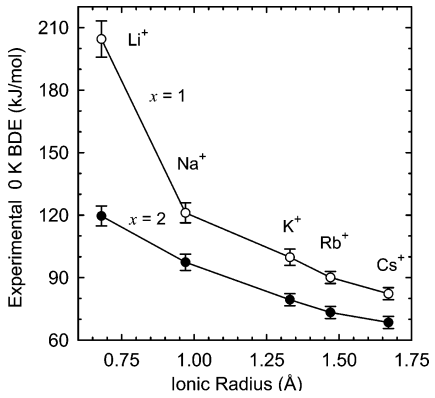

Figure 7. Bond dissociation energies at 0 K (in kJ/mol) of the $M^+(C_8H_7N)_x$ complexes plotted vs the ionic radius of M^+. Data are shown for $x = 1$ and 2 as ○ and ●, respectively. All values are taken from Table 2.

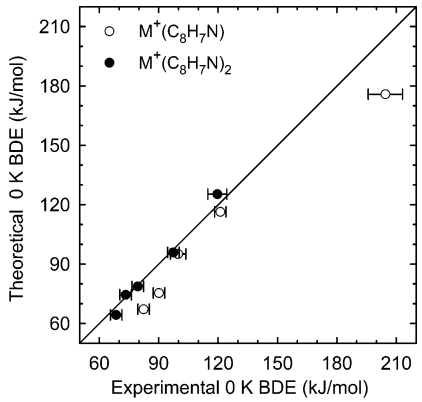

Figure 8. Theoretical versus experimental 0 K bond dissociation energies of $M^+-(C_8H_7N)$ and $(C_8H_7N)M^+-(C_8H_7N)$ (in kJ/mol), where $M^+ = Li^+$, Na^+, K^+, Rb^+, and Cs^+. Data are shown for $x = 1$ and 2 as ○ and ●, respectively.

reasonable to think of the $M^+(C_8H_7N)_2$ complexes as highly dynamical structures with the alkali metal cation interacting with the phenyl rings of both ligands.

Conformations of the bis-complexes in which the alkali metal cation binds to the pyrrolyl ring via a π5-type interaction can also be envisioned but are expected to be less stable than the π6 conformers. Attempts to calculate such structures always converged to an energetically more favorable conformation in which the alkali metal cation binds to the phenyl rings of both indole ligands except for the $Li^+(C_8H_7N)_2$ complex, where we found a low-energy conformer, designated here as π5a, in which Li^+ binds to the phenyl ring of one indole ligand and the pyrrolyl ring of the other indole ligand. The indole ligands orient themselves, in a "near anti" configuration, so that the unbound rings of the two indole ligands are oriented as far apart as possible to minimize ligand−ligand repulsive interactions.

Conversion from 0 to 298 K. To allow comparison to literature values and commonly used experimental conditions, we convert the 0 K BDEs determined here to 298 K bond enthalpies and free energies. The conversions are calculated using standard formulas (assuming harmonic oscillator and rigid rotor models) and the vibrational and rotational constants determined for the B3LYP/6-31G* optimized geometries, listed in Table 1S and 2S. Table 4S lists the 0 and 298 K enthalpy, free energy, and enthalpic and entropic corrections for all systems experimentally and theoretically determined (from Table 2). Uncertainties are determined by 10% variation in the molecular constants.

Discussion

Trends in the Experimental $M^+(C_8H_7N)_x$ BDEs. The 0 K experimental BDEs of the $M^+(C_8H_7N)_x$ complexes are summarized in Table 2. The variation in the measured BDEs with the size of the alkali metal cation is shown in Figure 7 for both the mono- and bis-complexes. The $M^+-(C_8H_7N)$ and (C_8H_7N)-$M^+-(C_8H_7N)$ BDEs are found to decrease monotonically as the size of the alkali metal cation increases from Li^+ to Cs^+. Similar behavior was observed for cation−π complexes involving other aromatic ligands previously studied.[26,28−35] This behavior supports the conclusion that these complexes are noncovalently bound. The BDEs decrease with increasing size of the alkali metal cation because the distance between the alkali metal cation and the aromatic ligand is largely determined by the size of the cation (Table 3). The larger the radius of the alkali metal cation, the longer the alkali metal cation−indole bond distance and thus the weaker the interaction.

The BDEs of the bis-complexes are smaller than the corresponding mono-complexes in all cases. The difference in BDEs is largest for Li^+ and decreases with increasing size of the alkali metal cation. The sequential BDEs are found to decrease by 84.9, 23.7, 23.6, 16.8, and 13.8 kJ/mol for the Li^+, Na^+, K^+, Rb^+, and Cs^+ complexes, respectively. The more rapid fall off observed for the smaller cations can be explained in terms of Coulombic and dipole−dipole repulsions between the two indole ligands. The distance between the two ligands increases with the size of alkali metal cation from 4.08 Å in $Li^+(C_8H_7N)_2$ to 6.91 Å in $Cs^+(C_8H_7N)_2$ (Table 3, $2 \times M^+-R_\perp$ distance of the π6a conformers). Thus, the magnitude of the repulsive forces should decrease with increasing separation of the two ligands. This results in smaller differences in the BDEs for the mono- and bis-complexes as the size of the alkali metal cation increases.

Comparison of Theory and Experiment. The experimentally measured and theoretically calculated BDEs of the $M^+(C_8H_7N)_x$ complexes are summarized in Table 2, while the agreement between theory and experiment is illustrated in Figure 8. As can be seen in the figure, the agreement is very good for the Li^+, Na^+, and K^+ complexes, where full electron correlation is included, except for the $Li^+(C_8H_7N)$ complex. Slightly poorer agreement between theory and experiment is found for the Rb^+ and Cs^+ complexes, where ECPs are employed. The mean absolute deviation (MAD) between the experimental and theoretical values for all 10 $M^+(C_8H_7N)_x$ complexes is 8.1 ± 8.9 kJ/mol, somewhat larger than the average experimental error (AEE), 3.8 ± 1.8 kJ/mol. The MAD is larger for the mono-complexes, 13.6 ± 9.9 kJ/mol, than for the bis-complexes, 2.7 ± 2.2 kJ/mol. The agreement between the experimental and six theoretical BDEs calculated including all electrons ($M^+ = Li^+$, Na^+, K^+ and $x = 1$ and 2) is reasonably good, with a MAD of 7.7 ± 10.5 kJ/mol, again somewhat larger than the average experimental error in these values, 4.4 ± 2.3 kJ/mol. The large difference in the experimental and theoretical BDE for the $Li^+(C_8H_7N)$ complex is the major contributor to the MADs. If this value is not included, the MAD for the nine complexes drops to 5.8 ± 5.4 kJ/mol, much closer to the AEE of 3.2 ± 0.7 kJ/mol and the accuracy expected for the level of theory employed here (~8 kJ/mol).[25] The poor agreement for the $Li^+(C_8H_7N)$ complex most likely arises because the basis sets employed for Li^+ do not allow effective core polarization. Results of another study currently being conducted in our laboratory suggest that core polarization is very important for an accurate description of Li^+−ligand interactions.[90] Thus, the measured BDE of the $Li^+(C_8H_7N)$ complex is expected to be more reliable than the theoretical value calculated here.

The agreement between the experimental BDEs and the theoretical values calculated using the Hay−Wadt ECP/valence basis set for the Rb^+ and Cs^+ complexes is also reasonably good. A MAD of 8.8 ± 7.2 kJ/mol is found, somewhat larger than the AEE in these values, 2.9 kJ/mol. Consistent with previous studies of other cation−π complexes,[26,29−35] the Hay−Wadt ECP/valence basis set provides calculated BDEs that are reasonably accurate but systematically lower than the experimental values.

Comparison to Literature Theoretical Values. Previous theoretical studies of the alkali metal cations binding to indole have been limited to Na^+ and K^+. Mecozzi, West, and Dougherty calculated the binding energy of Na^+ to a variety of model π ligands including indole at the HF/6-31G** level of theory and showed that the variation in the binding energies of these ligands could be rationalized in terms of an electrostatic model. The binding energy of Na^+ to indole (D_e) was calculated to be 136.5 kJ/mol, only 4.7 kJ/mol higher than that calculated here. To determine the effects of ZPE and BSSE corrections on the calculated binding energy, we repeated this calculation and included ZPE and BSSE corrections and found that at this level of theory D_0 = 132.2 kJ/mol, 4.8 kJ/mol higher than that calculated here, and $D_{0,BSSE}$ = 125.4 kJ/mol, 9.0 kJ/mol higher than that calculated here. Thus, inclusion of MP2 correlation and a larger basis set for the single point energy calculation leads to a moderate decrease in the calculated binding energy. Later, Dunbar calculated the binding energy of Na^+ to indole (D_e) at the MP2/6-31G*//HF/6-31G* level of theory to be 150.6 kJ/mol, 18.8 kJ/mol higher than that calculated here.[49] Because they were only interested in mapping the potential energy surface (PES) rather than obtaining absolute binding energies, ZPE and BSSE corrections were again not included and a frozen HF geometry for indole was employed. The BDE difference between binding to the phenyl ring and pyrrolyl ring was found to be 16.8 kJ/mol, similar to that found here, 12.3 kJ/mol. The MP2(full)/6-311+G(2d,2p)//MP2(full)/6-31G* theory employed in the present work provides a BDE for $Na^+(C_8H_7N)$ of 116.4 kJ/mol, in good agreement with measured value 121.1 ± 2.9 kJ/mol. Therefore, it is obvious that to determine accurate theoretical BDEs, full optimization of the complex, full MP2 correlation, and ZPE and BSSE corrections should be included, although BSSE corrections are more important for ab initio calculations than for density functional theory calculations.

Influence of the Metal Cation on Binding to Indole. As discussed above, the strength of the binding in the $M^+(C_8H_7N)_x$ complexes varies with both the alkali metal cation and the extent of ligation. In addition, the stable conformations found for these complexes also vary with the alkali metal cation. Stable minima of the $M^+(C_8H_7N)$ complexes are found for all five alkali metal cations binding to the phenyl ring, whereas stable binding to the pyrrolyl ring is found only for Li^+, Na^+, and K^+. Similarly, the stable minima found for the $M^+(C_8H_7N)_2$ complexes always involve binding of both ligands to the phenyl rings, except for the $Li^+(C_8H_7N)_2$ complex where an additional low-energy conformer is found in which one of the indole ligands binds via the phenyl ring while the other binds via the pyrrolyl ring. These results suggest that the PES for interaction with the π face of indole is a double-well potential and that the energy barrier between these wells is small and dependent upon the alkali metal cation. The relaxed potential energy scans for the interconversion of the π6 and π5 conformers of Li^+, Na^+, and K^+ support this conclusion and are shown in Figure 6. As can be seen in the figure, the barrier to interconversion is greatest for Li^+ and essentially disappears for Na^+ and K^+. On the basis of the shape of these reaction coordinate diagrams it is somewhat surprising that a π5 minimum was even found for Na^+ and K^+ and not surprising that the TS between the π6 and π5 conformers could not be found for these alkali metal cations. Extrapolation of these results to Rb^+ and Cs^+ also explains why no stable π5 minima were found for these alkali metal cations.

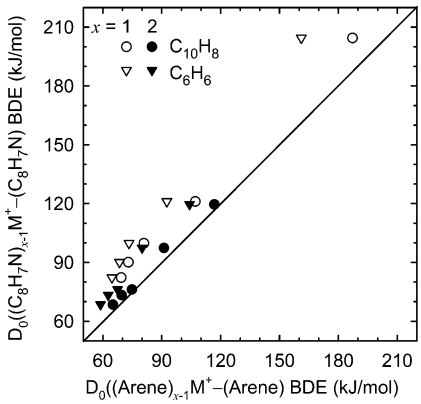

Figure 9. Bond dissociation energies of $(C_8H_7N)_{x-1}M^+-(C_8H_7N)$ vs $(Arene)_{x-1}M^+-(Arene)$ at 0 K (in kJ/mol), where $M^+ = Li^+$, Na^+, K^+, Rb^+, and Cs^+ and. Data are shown for Arene = C_6H_6 and $C_{10}H_8$ and x = 1 as ▽ and ○ and for x =2 as ▼ and ●, respectively. Values for the $M^+(C_6H_6)_x$ and $M^+(C_{10}H_8)_x$ complexes are taken from refs 26 and 35, respectively.

The conclusion that the PES for interaction with the π face of indole is a double-well potential with an energy barrier that is dependent upon the metal cation was first suggested by Dunbar in an earlier theoretical study where he examined the binding of Na^+, Mg^+, and Al^+ to the π face of indole.[49] In that work he found that the energy barrier decreased as the size of the metal cation increased from Al^+ to Mg^+ to Na^+. In contrast, the calculated BDEs for these complexes follow the order $Na^+ < Al^+ < Mg^+$. This suggests that the distance between the metal cation and the π surface of indole, rather than the strength of the interaction, is the most important factor in determining whether the PES exhibits a single- or double-well potential and in the latter case the barrier to interconversion of the π6 and π5 conformers.

Influence of the Extended π Network and Nitrogen Heteroatom. To examine the effect of size of π network and the influence of the nitrogen heteroatom on the strength of cation−π interaction in the alkali metal cation−indole complexes, the present results are compared to the analogous complexes to benzene[26] and naphthalene.[35] Benzene is chosen for this comparison because the preferred binding site in the complexes to indole is above the phenyl ring, whereas naphthalene is chosen because the size of the π networks are similar. The measured BDEs of these ligands to the alkali metal cations are compared in Table 2 and Figure 9. As can be seen in the table and figure, the BDEs follow the order benzene < naphthalene < indole for all alkali metal cations in both the mono- and bis-complexes. The enhancement in the BDEs is greater for the mono-complexes than for the corresponding bis-complexes. Indole binds more strongly than benzene by 17.7−43.4 kJ/mol in the mono-complexes and 8.7−15.4 kJ/mol in the bis-complexes, corresponding to an average increase of 30.8 ± 3.8% and 15.4 ± 1.6%, respectively. Similarly, indole binds more strongly than naphthalene by 13.0−18.9 kJ/mol in the mono-complexes and 1.4−3.7 kJ/mol in the bis-complexes, corresponding to an average increase of 17.7 ± 6.2% and 3.3 ± 1.8%, respectively. The absolute enhancement in the binding is greatest for the Li^+ complexes and decreases with increasing size of the alkali metal cation.

In earlier studies Dougherty and co-workers showed that for nonpolarizable cations, e.g., alkali metal cations, the strength of the cation−π interaction is correlated to the charge-permanent quadrupole term of the molecular electrostatic potential. Later, Cubero et al.[91] showed that polarization (i.e., ion-induced dipole interactions) is also important to the binding. In principle, ion−dipole interactions could play a role as well. However, benzene and naphthalene have a center of symmetry and therefore no dipole moment, and the dipole moment of indole lies in the plane of the molecule, and thus ion−dipole interactions do not directly contribute to the binding. Instead, the effect of the in-plane dipole moment is to enhance the quadrupole moment of indole.

The quadrupole moment of benzene has been measured as ~8.69 D Å.[92] However, the quadrupole moment of naphthalene has not been reported but is expected to be similar to that of benzene.[35] In addition, the quadrupole moment of indole cannot be measured because the experimental technique for measuring the permanent quadrupole moment requires that the molecule have no dipole moment. However, the positive charge accumulated on the nitrogen atom of the pyrrolyl ring pushes electron density toward the phenyl ring and is therefore expected to enhance its quadrupole moment and the strength of the ion−quadrupole interaction in the alkali metal cation−indole complexes. Thus, the ion−quadrupole interaction in these systems is expected to follow the order benzene ≤ naphthalene < indole. The additivity method of Miller[58] provides estimated polarizabilities of 9.99, 17.59, and 15.35 Å^3 for benzene, naphthalene, and indole, respectively. Therefore, the ion-induced dipole interactions to indole should be stronger than to benzene and weaker than to naphthalene. Therefore, the ion-induced dipole interaction in these systems is expected to follow the order benzene < indole < naphthalene.

These simple comparisons suggest that the extended π networks of naphthalene and indole lead to stronger cation−π binding as compared to benzene as a result of enhancements in the ion-induced dipole interactions, whereas the nitrogen heteroatom of indole leads to stronger cation−π binding as compared to benzene and naphthalene as a result of enhancement in the ion−quadrupole interaction.

Trends in Binding of Alkali Metal Cations to the Aromatic Amino Acids, Phe, Tyr, and Trp versus Their Side-Chain Analogues: Benzene, Phenol, and Indole. The BDEs of cation−π complexes between the alkali metal cations and benzene (C_6H_6)[26] and phenol (C_6H_5OH)[33] are also given in Table 2. As can been seen in the table, the BDEs of the alkali metal complexes to benzene, phenol, and indole follow the order M^+-(C_6H_6) < M^+(C_6H_5OH) < M^+(C_8H_7N) for all of the alkali metal cations. The differences in the measured BDEs to benzene and phenol are small and generally smaller than the experimental error in these measurements, suggesting that the relative binding affinities of benzene and phenol may not be accurately known. However, competitive dissociation of M^+(C_6H_6)(C_6H_6OH) complexes clearly indicates that the binding to phenol is stronger than that to benzene.[93]

The polarizability of benzene is estimated to be 9.99 Å^3 and increases to 11.00 Å^3 for phenol and to 15.35 Å^3 for indole. As can be seen in Figure 10, a linear correlation between the measured BDEs and the estimated polarizabilities of these neutral π ligands is also found for all five alkali metal cations, supporting the conclusion that the polarizability of the π ligand is a key factor in determining the strength of the binding in cation−π complexes as previously suggested.[29−31,33−35,38,91]

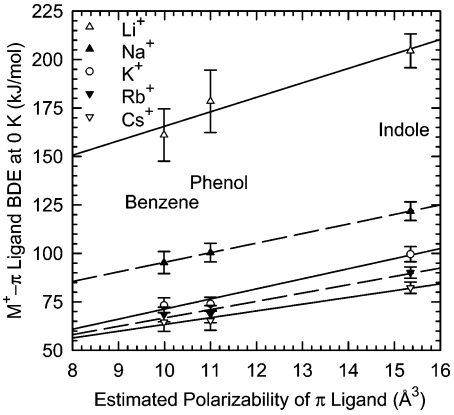

Figure 10. Measured $M^+-\pi$ ligand BDEs at 0 K (in kJ/mol) versus estimated polarizability[51] of the π ligand. Values are shown for M^+ = Li^+, Na^+, K^+, Rb^+, and Cs^+, and π ligand = benzene, phenol, and indole. Values for benzene and phenol are taken from refs 26 and 33, respectively. Lines are linear regression fits to the data for each alkali metal cation.

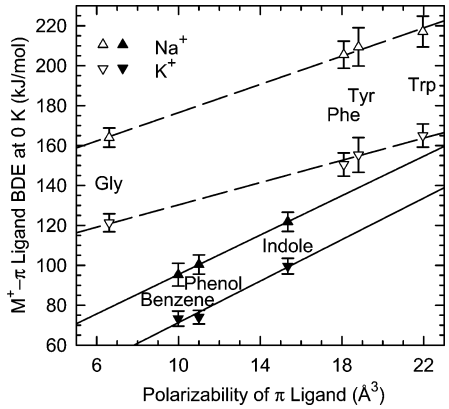

Figure 11. Measured $M^+-\pi$ ligand BDEs at 0 K (in kJ/mol) versus estimated polarizability[58] of the π ligand. Values are shown for M^+ = Na^+ and K^+ and π ligand = Gly, Phe, Tyr, Trp, benzene, phenol, and indole. Values for Gly are taken from refs 94 and 95, Phe, Tyr, and Trp are taken from ref 38, while values for benzene and phenol are taken from refs 26 and 33, respectively. Lines are linear regression fits to the data for each alkali metal cation and series of π ligands.

The trends in the calculated and measured BDEs for Na^+ and K^+ binding to the aromatic amino acids parallel that found for their side-chain analogues, i.e., the BDEs follow the order M^+(Phe) < M^+(Tyr) < M^+(Trp).[36−39] The binding in these complexes involves interaction with both the amino acid backbone and the side-chain substituent. Comparisons of the geometries and BDEs of these complexes to those for M^+-(Gly),[94,95] M^+(C_6H_6), M^+(C_6H_5OH), and M^+(C_8H_7N) suggested that the binding in the complexes to the aromatic amino acids is dominated by the interaction with the amino acid backbone and enhanced by interaction with the side-chain substituent.[38] As can been seen in Figure 11, the correlation between the binding energies and estimated polarizabilities is very different for the amino acids than for their aromatic side-chain analogues. The fact that the BDEs to the side-chain analogues increase more rapidly with polarizability than for the complexes to the aromatic amino acids suggests that the ion−quadrupole interaction plays a larger role in the former complexes. This again supports the conclusion that the binding in the complexes to the isolated aromatic amino acids is dominated by the amino acid backbone and enhanced by interaction with the aromatic side chain.

Indole as a Versatile π Donor in Biological Systems. As discussed in the Introduction, indole as the side-chain substituent

of Trp is involved in a wide variety of biological processes. The roles that Trp fulfills in these biological systems are all believed to involve cation−π interactions with the indole side-chain substituent. As found by Gallivan and Dougherty,[50] Trp is involved in energetically significant cation−π interactions more frequently than Phe and Tyr. They suggested that this preference might be attributed to either the stronger binding of cations by Trp as compared to Phe and Tyr or possibly the larger π surface of Trp, which might allow it to contact a greater number of cations relative to Phe or Tyr. They concluded that the preference for Trp over Phe and Tyr was attributable to the stronger binding, not to the larger volume of Trp, because it is less represented than Tyr in cation−π interacting pairs of amino acids. However, their conclusion was based upon analysis of static protein structures found in the protein data bank. Their analysis did not include any provision for changes in the conformations of these proteins during biological processes. The fact that indole as the side-chain substituent of Trp provides a large π surface for interaction with cations and that binding to the pyrrolyl ring is nearly as strong as to the phenyl ring suggests that the strength of cation−π interactions to Trp would not be significantly compromised when the protein undergoes changes in conformation associated with performing its biological function. Similarly, Tyr is over-represented in cation−π interactions as compared to Phe, 14.3% versus 10.0%. This difference is not likely to be attributable to energetic preferences because the cation-binding ability of Tyr is only slightly greater than that of Phe.[36,38,39] However similar to indole, phenol provides two strong cation-binding sites of similar binding affinity, the phenyl ring and the hydroxyl substituent. Therefore, the preference for Tyr over Phe in cation−π interactions is most likely attributable to its ability to bind cations to both sites, again providing a means by which the strength of noncovalent interactions with the side-chain substituent might not be significantly compromised upon conformational changes that occur during biological processes. Thus, we conclude that the preference for Trp over Phe and Tyr derives from both energetic and geometric considerations. Trp is over-represented because it is the strongest cation binder of these amino acids and provides for a versatile binding geometry that may be necessary to maintain the delicate balance of weak noncovalent interactions that control the complex three-dimensional structure of biological macromolecules.

Conclusions

The kinetic-energy dependences of the CID of $M^+(C_8H_7N)_x$ complexes, where $M^+ = Li^+$, Na^+, K^+, Rb^+, and Cs^+ and $x = 1$ and 2, with Xe are examined in a guided ion beam tandem mass spectrometer. The dominant pathway observed for all complexes is loss of an intact indole ligand. The thresholds for these primary dissociation reactions are interpreted to extract 0 and 298 K bond dissociation energies. The molecular parameters needed for the analysis of experimental data as well as structures and theoretical estimates of the BDEs for the $M^+(C_8H_7N)_x$ complexes are obtained from theoretical calculations performed at the MP2(full)/6-311+G(2d,2p)//B3LYP/6-31G* level of theory. The agreement between theory and experiment is reasonably good for all complexes except $Li^+(C_8H_7N)$, where theory underestimates the strength of the binding. The absolute $M^+-(C_8H_7N)$ and $(C_8H_7N)M^+-(C_8H_7N)$ BDEs are observed to decrease monotonically as the size of the alkali metal cation increases from Li^+ to Cs^+. Similarly, the differences in the BDEs for the mono- and bis-complexes are also observed to decrease with the size of the alkali metal cation. These trends confirm the electrostatic nature of the bonding in these $M^+(C_8H_7N)_x$ complexes.

Comparison of the present results to those obtained for the analogous complexes to benzene and naphthalene reveal that the primary effect of the extended π networks of naphthalene and indole is to increase the strength of cation binding via an enhancement in the ion-induced dipole interactions. In contrast, the effect of the nitrogen heteroatom of indole leads to stronger cation−π binding as a result of enhancement in the ion−quadrupole interaction. In addition, these comparisons provide a means by which the quadrupole moment of indole was estimated to be -11.2 ± 0.4 D Å. Comparison of the present results to those obtained for the analogous complexes to benzene and phenol reveal that the binding in these complexes correlates linearly with the quadrupole moments and polarizabilities of these aromatic ligands. In addition, the trends observed in the BDEs to these aromatic ligands parallel that to the corresponding isolated aromatic amino acids even though the binding in the latter complexes is dominated by interactions with the amino acid backbone. Finally, we conclude that Trp is over-represented in cation−π interactions operative in biological systems because it binds more strongly than Phe and Tyr and is a versatile cation binder, whose strength of interaction is not significantly compromised when the optimum binding geometry cannot be maintained as may occur during conformational changes that take place when biological macromolecules perform their various functions.

Acknowledgment. This work is supported by the National Science Foundation, Grant CHE-0518262, and the American Chemical Society Petroleum Research Fund, Grant 40334-AC6.

Supporting Information Available: Tables of vibrational frequencies and average vibrational energies at 298 K, rotational constants, B3LYP/6-31G*-optimized geometries, and enthalpies and free energies at 298 K; figures giving cross sections for collision-induced dissociation and thermochemical analyses of collision-induced dissociation cross sections (PDF). This material is available free of charge via the Internet at http://pubs.acs.org.

References and Notes

(1) Dougherty, D. A. *Science* **1996**, *271*, 163.
(2) Ma, J. C.; Dougherty, D. A. *Chem. Rev.* **1997**, *97*, 1303.
(3) Mecozzi, S.; West, A. P., Jr.; Dougherty, D. A. *J. Am. Chem. Soc.* **1996**, *118*, 2307.
(4) Mecozzi, S.; West, A. P., Jr.; Dougherty, D. A. *Proc. Natl. Acad. Sci. U.S.A.* **1996**, *93*, 10566.
(5) Gallivan, J. P.; Dougherty, D. A. *Proc. Natl. Acad. Sci. U.S.A.* **1999**, *96*, 9459.
(6) Nicholson, H.; Becktel, W. J.; Matthew, B. W. *Nature* **1988**, *336*, 651.
(7) Sancho, J.; Serrano, L.; Fersht, A. R. *Biochemistry* **1992**, *31*, 2253.
(8) Burley, S. K.; Petsko, G. A. *Science* **1985**, *34*, 15301.
(9) Serrano, L.; Bycroft, M.; Fesht, A. R. *J. Mol. Biol.* **1991**, *218*, 465.
(10) Sunner, J.; Nishizawa, K.; Kebarle, P. *J. Phys. Chem.* **1981**, *85*, 1814.
(11) Meotner, M.; Deakyne, C. A. *J. Am. Chem. Soc.* **1985**, *107*, 469.
(12) Deakyne, C. A.; Meotner, M. *J. Am. Chem. Soc.* **1985**, *107*, 474.
(13) Guo, B. C.; Purnell, J. W.; Castleman, A. W. *Chem. Phys. Lett.* **1990**, *168*, 155.
(14) Carbarcos, O. M.; Weinheimer, C. J.; Lisy, J. M. *J. Chem. Phys.* **1998**, *108*, 5151.
(15) Devos, A. M.; Ultsch, M.; Kossiakoff, A. A. *Science* **1992**, *255*, 306.
(16) Karlin, A. *Curr. Opin. Neurobiol.* **1993**, *3*, 299.
(17) Stauffer, D. A.; Karlin, A. *Biochemistry* **1994**, *33*, 6840.
(18) Mitchell, J. B.; Nandi, C. L.; McDonald, I. K.; Thornton, J. M.; Price, S. L. *J. Mol. Biol.* **1994**, *239*, 315.

(19) Raves, M. L.; Harel, M.; Pang, Y. P.; Silman, I.; Kozikowski, A. P.; Sussman, J. L. *Nat. Struct. Biol.* **1997**, *4*, 57.
(20) Zhong, W.; Gallivan, J. P.; Zhang, Y.; Li, L.; Lester, H. A.; Dougherty, D. A. *Proc. Natl. Acad. Sci. U.S.A.* **1998**, *95*, 12088.
(21) Donini, O.; Weaver, D. F. *J. Comput. Chem.* **1998**, *19*, 1515.
(22) Cabarcos, O. M.; Weinheimer, C. J.; Lisy, J. M. *J. Chem. Phys.* **1999**, *110*, 8429.
(23) Woodin, R. L.; Beauchamp, J. L. *J. Am. Chem. Soc.* **1978**, *100*, 501.
(24) Taft, R. W.; Anvia, F.; Gal, J.-F.; Walsh, S.; Capon, M.; Holmes, M. C.; Hosn, K.; Oloumi, G.; Vasanwala, R.; Yazdani, S. *Pure Appl. Chem.* **1990**, *62*, 17.
(25) Armentrout, P. B.; Rodgers, M. T. *J. Phys. Chem. A* **2000**, *104*, 2238.
(26) Amicangelo, J. C.; Armentrout, P. B. *J. Phys. Chem. A* **2000**, *104*, 11420.
(27) Gapeev, A.; Yang, C.-N.; Klippenstein, S. J.; Dunbar, R. C. *J. Phys. Chem. A* **2000**, *104*, 3246.
(28) Huang, H.; Rodgers, M. T. *J. Phys. Chem. A* **2002**, *106*, 4277.
(29) Amunugama, R.; Rodgers, M. T. *J. Phys. Chem. A* **2002**, 5529.
(30) Amunugama, R.; Rodgers, M. T. *J. Phys. Chem. A* **2002**, *106*, 9092.
(31) Amunugama, R.; Rodgers, M. T. *Int. J. Mass Spectrom.* **2003**, *227*, 339.
(32) Ryzhov, V.; Dunbar, R. C. *J. Am. Chem. Soc.* **1999**, *121*, 2259.
(33) Amunugama, R.; Rodgers, M. T. *J. Phys. Chem. A* **2002**, *106*, 9718.
(34) Amunugama, R.; Rodgers, M. T. *Int. J. Mass Spectrom.* **2003**, *222*, 431.
(35) Amunugama, R.; Rodgers, M. T. *Int. J. Mass. Spectrom.* **2003**, *227*, 1.
(36) Ryzhov, V.; Dunbar, R. C.; Cerda, B.; Wesdemiotis, C. *J. Am. Soc. Mass Spectrom.* **2000**, *11*, 1037.
(37) Gapeev, A.; Dunbar, R. C. *J. Am. Chem. Soc.* **2001**, *123*, 8360.
(38) Ruan, C.; Rodgers, M. T. *J. Am. Chem. Soc.* **2004**, *126*, 14600.
(39) Kish, M. M.; Ohanessian, G.; Wesdemiotis, C. *Int. J. Mass Spectrom.* **2003**, *227*, 509.
(40) Murayama, K.; Aoki, K. *Inorg. Chim. Acta* **1998**, *281*, 36.
(41) Gokel, G. W.; Wall, S. L.; Meadows, E. S. *Eur. J. Org. Chem.* **2000**, 2967.
(42) Zarric, S. D.; Popovic, D. M.; Knapp, E.-W. *Chem. Eur. J.* **2000**, *6*, 3935.
(43) Dunbar, R. C. *J. Phys. Chem. A* **2000**, *104*, 8067.
(44) Feller, D.; Dixon, D. A.; Nicholas, J. B. *J. Phys. Chem. A* **2000**, *104*, 11414.
(45) Tsuzuki, S.; Yoshida, M.; Uchimaru, T.; Mikami, M. *J. Phys. Chem. A* **2001**, *105*, 769.
(46) Miklis, P. C.; Ditchfield, R.; Spencer, T. A. *J. Am. Chem. Soc.* **1998**, *120*, 10482.
(47) Kim, K. S.; Lee, J. Y.; Lee, S. J.; Ha, T.-K.; Kim, D. H. *J. Am. Chem. Soc.* **1994**, *116*, 7399.
(48) Pullman, A.; Berthier, G.; Savinelli, R. *J. Am. Chem. Soc.* **1998**, *120*, 8553.
(49) Dunbar, R. C. *J. Phys. Chem. A* **1998**, *102*, 8946.
(50) Gallivan, J. P.; Dougherty, D. A. *Proc. Natl. Acad. Sci. U.S.A.* **1999**, *96*, 9459.
(51) Landolt-Marticorena, C.; Williams, K. A.; Deber, C. M.; Reithmeier, R. A. F. *J. Mol. Biol.* **1993**, *229*, 602.
(52) Ulmschnider, M. D.; Sansom, M. S. P. *Biochim. Biophys. Acta* **2001**, *1512*, 1.
(53) Clark, E. H.; East, M. J.; Lee, A. G. *Biochemistry* **2003**, *42*, 11065.
(54) Dougherty, D. A.; Stauffer, D. A. *Science* **1990**, *250*, 4987.
(55) Schiefner, A.; Breed, J.; Bosser, L.; Kneip, S.; Gade, J.; Holtmann, G.; Diederichs, K.; Welte, W.; Bremer, E. *J. Biol. Chem.* **2004**, *279*, 5588.
(56) Koerner, C.; Guan, T.; Gerace, L.; Cingolani, G. *J. Biol. Chem.* **2003**, *278*, 16216.
(57) Kagan, R. M.; Clarke, A. *Biochem. Biophys.* **1994**, *310*, 417.
(58) Miller, K. J. *J. Am. Chem. Soc.* **1990**, *112*, 8533.
(59) Rodgers, M. T.; Ervin, K. M.; Armentrout, P. B. *J. Chem. Phys.* **1997**, *106*, 4499.
(60) Rodgers, M. T. *J. Phys. Chem. A* **2001**, *105*, 2374.
(61) Teloy, E.; Gerlich, D. *Chem. Phys.* **1974**, *4*, 417.
(62) Gerlich, D. Diplomarbeit, University of Freiburg, Federal Republic of Germany, 1971.
(63) Gerlich, D. In *State-Selected and State-to-State Ion−Molecule Reaction Dynamics, Part I, Experiment*; Ng, C.-Y., Baer, M., Eds.; Advances in Chemical Physics Series; Wiley: New York, 1992; Vol. 82, p 1.
(64) Hales, D. A.; Armentrout, P. B. *J. Cluster Sci.* **1990**, *1*, 127.
(65) Dalleska, N. F.; Honma, K.; Armentrout, P. B. *J. Am. Chem. Soc.* **1993**, *115*, 12125.
(66) Aristov, N.; Armentrout, P. B. *J. Phys. Chem.* **1986**, *90*, 5135.
(67) Ervin, K. M.; Armentrout, P. B. *J. Chem. Phys.* **1985**, *83*, 166.
(68) Dalleska, N. F.; Honma, K.; Sunderlin, L. S.; Armentrout, P. B. *J. Am. Chem. Soc.* **1994**, *116*, 3519.
(69) Frisch, M. J.; Trucks, G. W.; Schlegel, H. B.; Scuseria, G. E.; Robb, M. A.; Cheeseman, J. R.; Zakrzewski, V. G.; Montgomery, J. A., Jr.; Stratmann, R. E.; Burant, J. C.; Dapprich, S.; Millam, J. M.; Daniels, A. D.; Kudin, K. N.; Strain, M. C.; Farkas, O.; Tomasi, J.; Barone, V.; Cossi, M.; Cammi, R.; Mennucci, B.; Pomelli, C.; Adamo, C.; Clifford, S.; Ochterski, J.; Petersson, G. A.; Ayala, P. Y.; Cui, Q.; Morokuma, K.; Malick, D. K.; Rabuck, A. D.; Raghavachari, K.; Foresman, J. B.; Cioslowski, J.; Ortiz, J. V.; Stefanov, B. B.; Liu, G.; Liashenko, A.; Piskorz, P.; Komaromi, I.; Gomperts, R.; Martin, R. L.; Fox, D. J.; Keith, T.; Al-Laham, M. A.; Peng, C. Y.; Nanayakkara, A.; Gonzalez, C. Challacombe, M.; Gill, P. M.; Replogle, E. S.; Pople, J. A. *Gaussian 98*, Revision A.11; Gaussian, Inc.: Pittsburgh, PA, 1998.
(70) Lee, C.; Yang, W.; Parr, R. G. *Phys. Rev. B* **1988**, *37*, 785.
(71) Becke, A. D. *J. Chem. Phys.* **1993**, *98*, 5648.
(72) Hay, P. J.; Wadt, W. R. J. *Chem. Phys.* **1985**, *82*, 299.
(73) Glendening, E. D.; Feller, D.; Thompson, M. A. *J. Am. Chem. Soc.* **1994**, *116*, 10657.
(74) Scott, A. P.; Radom, L. *J. Phys. Chem.* **1996**, *100*, 16502.
(75) Wong, M. W. *Chem. Phys. Lett.* **1996**, *256*, 391.
(76) Foresman, J. B.; Frisch, Æ. *Exploring Chemistry with Electronic Structure Methods*, 2nd ed.; Gaussian: Pittsburgh, PA, 1996.
(77) Boys, S. F.; Bernardi, R. *Mol. Phys.* **1979**, *19*, 553.
(78) van Duijneveldt, F. B.; van Duijneveldt-van de Rijdt, J. G. C. M.; van Lenthe, J. H. *Chem. Rev.* **1994**, *94*, 1873.
(79) Muntean, F.; Armentrout, P. B. *J. Chem. Phys.* **2001**, *115*, 1213.
(80) Beyer, T. S.; Swinehart, D. F. *Comm. Assoc. Comput. Machines* **1973**, *16*, 379.
(81) Stein, S. E.; Rabinovitch, B. S. *J. Chem. Phys.* **1973**, *58*, 2438.
(82) Stein, S. E.; Rabinovitch, B. S. *Chem. Phys. Lett.* **1977**, *49*, 183.
(83) Pople, J. A.; Schlegel, H. B.; Raghavachari, K.; DeFrees, D. J.; Binkley, J. F.; Frisch, M. J.; Whitesides, R. F.; Hout, R. F.; Hehre, W. J. *Int. J. Quantum Chem. Symp.* **1981**, *15*, 269.
(84) DeFrees, D. J.; McLean, A. D. *J. Chem. Phys.* **1985**, *82*, 333.
(85) Khan, F. A.; Clemmer, D. E.; Schultz, R. H.; Armentrout, P. B. *J. Phys. Chem.* **1993**, *97*, 7978.
(86) Chesnavich, W. J.; Bowers, M. T. *J. Phys. Chem.* **1979**, *83*, 900.
(87) See, for example, Figure 1 in Dalleska, N. F.; Honma, K.; Armentrout, P. B. *J. Am. Chem. Soc.* **1993**, *115*, 12125.
(88) Armentrout, P. B.; Simons, J. *J. Am. Chem. Soc.* **1992**, *114*, 8627.
(89) The $M^+-R_\perp$ distance is defined as the perpendicular distance between the alkali metal cation and the phenyl ring of indole, while the M^+-R_C distance is defined as the distance between the alkali metal cation and the centroid of the phenyl ring of indole.
(90) Rodgers, M. T.; Armentrout, P. B. Work in progress.
(91) Cubero, E.; Luque, F. J.; Orozco, M. *Proc. Natl. Acad. Sci. U.S.A.* **1998**, *95*, 5976.
(92) Williams, J. H. *Acc. Chem. Res.* **1993**, *26*, 593.
(93) Ditri, T. B.; Rodgers, M. T. Unpublished results.
(94) Moision, R. M.; Armentrout, P. B. *J. Phys. Chem. A* **2002**, *106*, 10350.
(95) Moision, R. M.; Armentrout, P. B. *Phys. Chem. Chem. Phys.* **2004**, *6*, 2588.